Research Square

Preprints are preliminary reports that have not undergone peer review.
They should not be considered conclusive, used to inform clinical practice,
or referenced by the media as validated information.

# Transport of Compensated Baryon-Asymmetry Domains in an Expanding Universe with Exact Spherical Diffusion and a Conditional Scalar-Field Test

**Syed Eirfan Atthar**

20wj1a03b1@gniindia.org

Dibrugarh University

**Research Article**

**Keywords:** baryon asymmetry, matter-antimatter domains, compensated configuration, FLRW cosmology, diffusion, scalar field, baryon isocurvature

**Posted Date:** November 3rd, 2026

**DOI:** https://doi.org/10.21203/rs.3.rs-11584440/v1

**License:** This work is licensed under a Creative Commons Attribution 4.0 International License.
Read Full License

**Additional Declarations:** No competing interests reported.

# Transport of Compensated Baryon-Asymmetry Domains in an Expanding Universe with Spherical Diffusion and a Conditional Scalar-Field Test

Syed Eirfan Atthar

Department of Mechanical Engineering, Specialization in Thermal and Fluid

Dibrugarh University Institute of Engineering and Technology (DUIET)

Dibrugarh University, Dibrugarh 786004, Assam, India

ORCID: 0009-0006-4126-6659

Corresponding author: Syed Eirfan Atthar

**Abstract**

This paper examines how diffusion changes a finite, globally compensated baryon-asymmetry profile in an expanding, spatially flat Friedmann-Lemaître-Robertson-Walker universe. Coupled baryon and antibaryon balance equations are reduced to an equation for the signed asymmetry, and the conditions for conservation of its spatial integral are stated. Using the accumulated comoving diffusivity, we derive the exact three-dimensional heat-kernel response for a spherical positive core surrounded by an oppositely signed shell whose amplitude is fixed by volume compensation. The resulting central-contrast function gives a 95% retention threshold that depends on the shell-to-core radius ratio. For a radius ratio of two, the dimensionless diffusion time must satisfy $I_D/R_c^2 \leq 0.06164$, compared with $0.13016$ for a planar step. At late times, cancellation of the monopole moment leads to a central decay proportional to $u^{-5/2}$. A separate conditional scalar-field benchmark, normalised to the baryon-to-photon ratio, gives $m_\phi = (5.073 \pm 0.016) \times 10^{-16}$ GeV for the stated parameters.

**Keywords:** baryon asymmetry; matter-antimatter domains; compensated configuration; FLRW cosmology; diffusion; scalar field; baryon isocurvature.

## 1 Introduction

The observable universe contains a substantial excess of baryons over antibaryons. The present baryon-to-photon ratio is very small, but its nonzero value has important consequences for the formation of nuclei, stars, galaxies, and the large-scale matter

distribution. The origin of this asymmetry remains an open problem in cosmology. Charge-parity violation has been observed in baryon decays, but that observation alone does not identify the mechanism responsible for the cosmic abundance [1]. Recent model-dependent proposals continue to connect baryogenesis with other early-Universe observables, including primordial magnetic fields [2]. Sakharov's conditions provide the basic requirements for a dynamical explanation: baryon-number violation, charge-conjugation and charge-parity violation, and a departure from thermal equilibrium [3]. These requirements have motivated electroweak baryogenesis, grand-unified mechanisms, Affleck-Dine models, spontaneous baryogenesis, and leptogenesis [4–9].

A separate question concerns whether the signed baryon excess can vary in space. Such profiles have been studied in the context of baryon isocurvature, scalar-field dynamics, inflation, nucleosynthesis, and annihilation radiation [10–19]. Their viability depends on the origin of the initial profile and its subsequent transport and annihilation history. Gamma-ray observations and cosmic-ray antinuclei searches provide further constraints, although their interpretation depends on astrophysical production and propagation models [20–23].

Recent work has continued to examine the evolution of antimatter domains in a baryon-asymmetric environment. Weiss and co-authors study domain survival, annihilation at the boundary, chemical evolution during the nucleosynthesis era, and the possible production of primordial antihelium-4 [24]. Earlier analyses by Khlopov and Lecian considered the evolution of dense domains in an expanding background, including boundary annihilation and possible nested structures [25]. Their related proceedings paper examined diffusion-length-based evolution and interactions in a spherical boundary shell [26]. The present work does not claim that spherical antimatter domains, diffusion, or boundary annihilation are new subjects. It addresses a more restricted question: after a signed source has switched off, how does linear diffusion change the central contrast of a finite, exactly compensated core-shell profile? This question can be answered for the specified initial condition without replacing the species-level reaction calculations used in studies of physical domain evolution. The result depends on the time integral of the proper diffusivity weighted by the inverse square of the scale factor, as well as on the geometry and compensation of the initial profile.

The contribution is an analytic transport result for a specified initial-value problem. It is not a replacement for the moving-boundary, species-level annihilation, or plasma-chemistry treatments in the earlier literature. The closed-form convolution is derived from the standard heat kernel; the quantities evaluated here are the compensation-dependent central-contrast function, its radius-ratio-dependent retention threshold, and

the coefficient of its late-time decay. These results should be read as a geometry-specific mathematical comparison, not as a claim that the full physical evolution of a primordial antimatter domain has been solved.

The planar diffusion problem provides a useful benchmark, but a finite spherical region has curvature and a finite compensation volume. A planar step therefore cannot be assumed to give the same retention condition as a finite spherical configuration. The main analytical contribution of this paper is an exact heat-kernel solution for a compensated spherical core-shell profile. From that solution we obtain a dimensionless central-contrast function, a numerical 95% retention threshold as a function of the shell-to-core radius ratio, and the late-time decay that follows when the net signed volume integral vanishes. The derivation uses the standard diffusion Green function [27], but the resulting expressions are applied here to a finite compensated baryon-asymmetry profile.

The paper also retains a conditional scalar-field source as a possible way of parameterising the local sign of the asymmetry. A derivative interaction with the baryon current is used in the effective form familiar from spontaneous-baryogenesis models [7, 28]. A quadratic potential is adopted for a transparent benchmark. The scalar profile is imposed as initial data. It is not generated by that potential, and the calculation is not presented as a new microscopic theory of baryogenesis. The observed baryon-to-photon ratio is used only to calibrate the source amplitude. Published cosmological constraints are used as reference values; no raw CMB, BBN, gamma-ray, or cosmic-ray catalogue is downloaded or analysed in this study.

The analysis has four objectives. First, it derives the signed-density transport equation and states the boundary and source conditions required for global compensation. Second, it gives the exact planar and spherical diffusion solutions and quantifies the central-contrast retention of a compensated core-shell profile. Third, it evaluates one conditional scalar-source benchmark against the published baryon abundance and the radiation energy density. Fourth, it presents an explicitly approximate isocurvature screen and a finite-duration stochastic estimate. These calculations test specified assumptions. They do not establish that the universe contains a primordial antimatter region, that its global baryon number is zero, or that the assumed initial profile is dynamically produced.

We adopt a spatially flat Friedmann-Lemaître-Robertson-Walker (FLRW) spacetime with line element

$$\mathrm{d}s^2 = -\,\mathrm{d}t^2 + a^2(t)\,\mathrm{d}\boldsymbol{\chi}^2, \tag{1}$$

where $a(t)$ is the scale factor and $\boldsymbol{\chi}$ is a comoving spatial coordinate. We use $c = 1$ in the spacetime equations. The Hubble parameter is $H = \dot{a}/a$. The background expansion is governed by the standard Friedmann equations. No modification of gravity is introduced, and antimatter is not assigned a negative gravitational mass. Laboratory measurements of antihydrogen are consistent with attractive gravitational acceleration within their reported precision [29].

Let $n_+(\boldsymbol{\chi}, t)$ and $n_-(\boldsymbol{\chi}, t)$ denote the physical number densities of baryons and antibaryons. In a diffusion approximation, their transport equations are written as

$$\frac{\partial n_+}{\partial t} + 3Hn_+ = \frac{D(t)}{a^2(t)}\nabla_\chi^2 n_+ - \langle\sigma v\rangle n_+ n_- + S_+(\boldsymbol{\chi}, t), \tag{2}$$

$$\frac{\partial n_-}{\partial t} + 3Hn_- = \frac{D(t)}{a^2(t)}\nabla_\chi^2 n_- - \langle\sigma v\rangle n_+ n_- + S_-(\boldsymbol{\chi}, t). \tag{3}$$

Here $D(t)$ is the proper diffusion coefficient, $\langle\sigma v\rangle$ is an effective pair-annihilation coefficient, and $S_\pm$ are source terms. The equations are phenomenological. A microscopic calculation of $D(t)$, $\langle\sigma v\rangle$, and the source rates is not attempted.

It is useful to define the signed and total densities,

$$\Delta n = n_+ - n_-, \qquad \Sigma n = n_+ + n_-. \tag{4}$$

Subtracting Eqs. (2) and (3) gives

$$\frac{\partial \Delta n}{\partial t} + 3H\Delta n = \frac{D(t)}{a^2(t)}\nabla_\chi^2 \Delta n + S_B, \qquad S_B = S_+ - S_-. \tag{5}$$

Adding the two equations gives

$$\frac{\partial \Sigma n}{\partial t} + 3H\Sigma n = \frac{D(t)}{a^2(t)}\nabla_\chi^2 \Sigma n - 2\langle\sigma v\rangle n_+ n_- + S_T, \qquad S_T = S_+ + S_-. \tag{6}$$

The explicit pair-annihilation term cancels from the signed equation because an idealised annihilation event removes one baryon and one antibaryon. It remains in the total-density equation. The cancellation is an identity of the adopted reaction term. It does not imply that annihilation is unimportant for the survival of a domain, since diffusion can bring opposite species into contact at an interface.

For an adiabatically expanding photon bath, $n_\gamma \propto a^{-3}$. Define the local baryon-to-photon asymmetry by

$$\eta(\boldsymbol{\chi}, t) = \frac{\Delta n(\boldsymbol{\chi}, t)}{n_\gamma(t)}. \tag{7}$$

If entropy production is negligible over the interval considered, the dilution terms cancel and Eq. (5) becomes

$$\frac{\partial \eta}{\partial t} = \frac{D(t)}{a^2(t)} \nabla_\chi^2 \eta + \frac{S_B}{n_\gamma}. \tag{8}$$

**Definition 1** (Global compensation)**.** *A signed-asymmetry configuration is globally compensated over a comoving region* $\Omega$ *if*

$$\int_\Omega a^3(t) \Delta n(\boldsymbol{\chi}, t)\, \mathrm{d}^3\chi = 0. \tag{9}$$

*For spatially uniform* $n_\gamma$*, this is equivalent to* $\int_\Omega \eta\, \mathrm{d}^3\chi = 0$*.*

**Proposition 1** (Conservation of the integrated signed density)**.** *Suppose that there is no diffusive flux through the boundary of* $\Omega$ *and that* $\int_\Omega S_B\, \mathrm{d}^3\chi = 0$ *at every time. Then the comoving integral* $a^3 \int_\Omega \Delta n\, \mathrm{d}^3\chi$ *is constant. In particular, an initially compensated configuration remains compensated even when its local signed density is nonzero.*

*Proof.* Multiply Eq. (5) by $a^3$ and integrate over $\Omega$. The derivative of $a^3$ cancels the dilution term $3H\Delta n$. The diffusion term reduces, by the divergence theorem, to a surface flux, which vanishes under the stated boundary condition. The integrated source also vanishes. Therefore

$$\frac{\mathrm{d}}{\mathrm{d}t} \left[ a^3(t) \int_\Omega \Delta n\, \mathrm{d}^3\chi \right] = 0. \tag{10}$$

□

For two approximately uniform regions with asymmetries $\eta_c$ and $\eta_s$, and volume fractions $f$ and $1-f$, compensation requires $f\eta_c + (1-f)\eta_s = 0$. Equal magnitudes of opposite sign follow only when the two volumes are equal. Compensation alone therefore does not prescribe equal domain sizes or equal local amplitudes.

## 2 Diffusion time and the planar reference solution

After the signed source has switched off, Eq. (8) reduces to

$$\frac{\partial \eta}{\partial t} = \frac{D(t)}{a^2(t)} \nabla_\chi^2 \eta. \tag{11}$$

Introduce the integrated comoving diffusivity

$$I_D(t; t_i) = \int_{t_i}^{t} \frac{D(t')}{a^2(t')}\, \mathrm{d}t'. \tag{12}$$

It has dimensions of comoving length squared. With $\tau = I_D$, Eq. (11) becomes the ordinary heat equation,

$$\frac{\partial \eta}{\partial \tau} = \nabla_\chi^2 \eta. \tag{13}$$

Thus the expansion history and the time dependence of the transport coefficient enter through a single accumulated quantity. An instantaneous value of $D(t)$ is not sufficient to determine the total amount of smoothing.

For a planar interface with initial data $\eta(\chi, t_i) = \eta_0 \,\mathrm{sgn}(\chi)$, the exact solution is

$$\eta(\chi, t) = \eta_0 \,\mathrm{erf}\left(\frac{\chi}{2\sqrt{I_D(t; t_i)}}\right). \tag{14}$$

At a comoving distance $R_c$ from the interface, the retained contrast is

$$C_{\mathrm{pl}}(R_c, t) = \frac{\eta(R_c, t)}{\eta_0} = \mathrm{erf}\left(\frac{R_c}{2\sqrt{I_D(t; t_i)}}\right). \tag{15}$$

For a required retained fraction $1 - \varepsilon$, with $0 < \varepsilon < 1$, the condition $C_{\mathrm{pl}} \geq 1 - \varepsilon$ is equivalent to

$$R_c \geq 2\sqrt{I_D(t; t_i)}\ \mathrm{erf}^{-1}(1 - \varepsilon). \tag{16}$$

At 95% retention, $\mathrm{erf}^{-1}(0.95) = 1.38590$, so that $R_c/\sqrt{I_D} \geq 2.77181$. This result is exact for the planar step and serves below as a geometric reference.

A simple expansion history illustrates the time dependence. Let

$$a(t) = a_i \left(\frac{t}{t_i}\right)^p, \qquad D(t) = D_i \left(\frac{t}{t_i}\right)^s. \tag{17}$$

Then

$$I_D(t; t_i) = \frac{D_i t_i}{a_i^2} \begin{cases} \dfrac{(t/t_i)^{s-2p+1} - 1}{s - 2p + 1}, & s - 2p + 1 \neq 0, \\ \ln(t/t_i), & s - 2p + 1 = 0. \end{cases} \tag{18}$$

The integral may converge or diverge at late times, depending on the transport law and the expansion exponent. No specific early-Universe diffusion law is imposed here.

For reference, define the local annihilation rate per particle by $\Gamma_{\mathrm{ann}} = \langle \sigma v \rangle n_{\mathrm{opp}}$, where $n_{\mathrm{opp}}$ is the density of the opposite species available for annihilation. A reaction-to-diffusion comparison on a physical scale $R_{\mathrm{phys}} = a R_c$ is

$$\mathrm{Da}_{\mathrm{ann}} = \frac{R_{\mathrm{phys}}^2 \Gamma_{\mathrm{ann}}}{D}. \tag{19}$$

A large value indicates that particles reaching an interface tend to react on a shorter timescale than the diffusion time across that scale. This parameter is a diagnostic only. Its value cannot be fixed without a microphysical calculation of the relevant densities and rates.

# 3 Exact diffusion of a compensated spherical core-shell profile

Consider a spherically symmetric initial asymmetry with a positive core of comoving radius $R_c$ and an opposite-sign shell extending to radius $R_s > R_c$:

$$\eta_i(r) = \eta_c\,\Theta(R_c - r) + \eta_s\,[\Theta(R_s - r) - \Theta(R_c - r)], \tag{20}$$

where $r = |\boldsymbol{\chi}|$, $\Theta$ is the Heaviside step function, and $\eta_c > 0$. The exterior is taken to have zero signed excess. The global compensation condition is

$$4\pi \int_0^\infty r^2 \eta_i(r)\,\mathrm{d}r = 0, \tag{21}$$

which gives

$$\eta_c R_c^3 + \eta_s(R_s^3 - R_c^3) = 0, \qquad \frac{\eta_s}{\eta_c} = -\frac{1}{q^3 - 1}, \qquad q = \frac{R_s}{R_c} > 1. \tag{22}$$

The shell amplitude is therefore fixed by the core and shell volumes. It is not an independent fitting parameter.

The Green function for Eq. (13) in three spatial dimensions is

$$G(\boldsymbol{r}, \tau) = \frac{1}{(4\pi\tau)^{3/2}} \exp\left(-\frac{|\boldsymbol{r}|^2}{4\tau}\right), \qquad \tau > 0. \tag{23}$$

Define the convolution of this kernel with a unit spherical top-hat of radius $R$ by

$$F(r, R, \tau) = \int_{|\boldsymbol{r}'|<R} G(\boldsymbol{r} - \boldsymbol{r}', \tau)\,\mathrm{d}^3 r'. \tag{24}$$

Performing the angular integration gives, for $r > 0$,

$$F(r,R,\tau) = \frac{1}{2}\left[\operatorname{erf}\left(\frac{R+r}{2\sqrt{\tau}}\right) + \operatorname{erf}\left(\frac{R-r}{2\sqrt{\tau}}\right)\right] - \frac{\sqrt{\tau}}{\sqrt{\pi}r}\left[\exp\left(-\frac{(R-r)^2}{4\tau}\right) - \exp\left(-\frac{(R+r)^2}{4\tau}\right)\right]. \tag{25}$$

The continuous central limit is

$$F(0,R,\tau) = \operatorname{erf}\left(\frac{R}{2\sqrt{\tau}}\right) - \frac{R}{\sqrt{\pi\tau}}\exp\left(-\frac{R^2}{4\tau}\right). \tag{26}$$

The expression tends to the unit top-hat as $\tau \to 0^+$ and is regular at the origin.

Using Eq. (22), the evolved compensated profile is

$$\eta(r,t) = (\eta_c - \eta_s)F(r,R_c,I_D) + \eta_s F(r,R_s,I_D) = \eta_c \frac{q^3 F(r,R_c,I_D) - F(r,R_s,I_D)}{q^3-1}. \tag{27}$$

This expression is exact for the stated top-hat core-shell initial condition and the diffusion equation in Eq. (11). It is not a numerical solution of a full baryon-antibaryon reaction network.

Introduce the dimensionless diffusion time

$$u = \frac{I_D(t;t_i)}{R_c^2}. \tag{28}$$

At the centre of the core, Eqs. (26) and (27) give

$$C_q(u) = \frac{\eta(0,t)}{\eta_c} = \frac{q^3 F_0(1,u) - F_0(q,u)}{q^3-1}, \tag{29}$$

where

$$F_0(z,u) = \operatorname{erf}\left(\frac{z}{2\sqrt{u}}\right) - \frac{z}{\sqrt{\pi u}}\exp\left(-\frac{z^2}{4u}\right). \tag{30}$$

For a chosen shell-to-core radius ratio, the 95% retention time $u_{95}$ is obtained from $C_q(u_{95}) = 0.95$. The values in Table 1 were calculated with a bracketed Brent root finder, using an absolute tolerance of $10^{-13}$. The closed form in Eq. (25) was checked against independent one-dimensional radial quadrature at representative radii and diffusion times, with absolute and relative integration tolerances of $10^{-11}$. The calculation evaluates the analytical model only; it does not use an observational data file. The numerical table is supplied in Online Resource the Python script used for the calculations and figures is supplied in the same.

**Table 1:** Numerical 95% central-contrast thresholds for compensated spherical core-shell profiles. The shell amplitude follows from exact volume compensation.

| $R_s/R_c$ | $\eta_s/\eta_c$ | $u_{95} = I_D/R_c^2$ | $R_c/\sqrt{I_D}$ at 95% |
|---|---|---|---|
| 1.25 | $-1.04918$ | 0.053765 | 4.31272 |
| 1.50 | $-0.42105$ | 0.058201 | 4.14510 |
| 2.00 | $-0.14286$ | 0.061636 | 4.02794 |
| 3.00 | $-0.03846$ | 0.063300 | 3.97464 |
| 5.00 | $-0.00806$ | 0.063835 | 3.95794 |
| 10.00 | $-0.00100$ | 0.063963 | 3.95398 |
| Planar step | n/a | 0.130159 | 2.77181 |

For $R_s/R_c = 2$, the central contrast falls below 95% when $I_D/R_c^2$ exceeds approximately 0.06164. The planar comparison allows a larger accumulated diffusion time, $I_D/R_c^2 \simeq 0.13016$, at the same nominal distance from the interface. The difference is expected: diffusion acts in all three spatial directions around a finite core, and the compensating shell contributes an opposite-sign component to the convolution. As the shell becomes larger relative to the core, its required amplitude decreases and the 95% threshold approaches the value for an isolated spherical top-hat. The threshold is not a universal domain-survival limit; it belongs to the specified initial geometry and to the signed-diffusion equation. The radial profiles at selected diffusion times are shown in Fig. 1. The dependence of the central contrast on dimensionless diffusion time, including the planar reference, is compared in Fig. 2.

The central solution also has a simple asymptotic form. The heat-kernel representation at the origin is

$$\eta(0,\tau) = \frac{1}{(4\pi\tau)^{3/2}} \int_{\mathbb{R}^3} \eta_i(r') \exp\left(-\frac{r'^2}{4\tau}\right) \mathrm{d}^3 r'. \tag{31}$$

For $\tau \gg R_s^2$, expand the exponential in powers of $1/\tau$. The leading term is proportional to the monopole integral $M_0 = \int \eta_i \, \mathrm{d}^3 r'$, which vanishes by compensation. The first nonzero contribution is controlled by the second radial moment,

$$M_2 = \int_{\mathbb{R}^3} r'^2 \eta_i(r') \, \mathrm{d}^3 r' = -\frac{4\pi}{5} \eta_c R_c^5 \frac{q^3(q^2-1)}{q^3-1}. \tag{32}$$

It follows that

$$C_q(u) = \frac{q^3(q^2-1)}{40\sqrt{\pi}(q^3-1)} u^{-5/2} + O(u^{-7/2}), \qquad u \gg q^2. \tag{33}$$

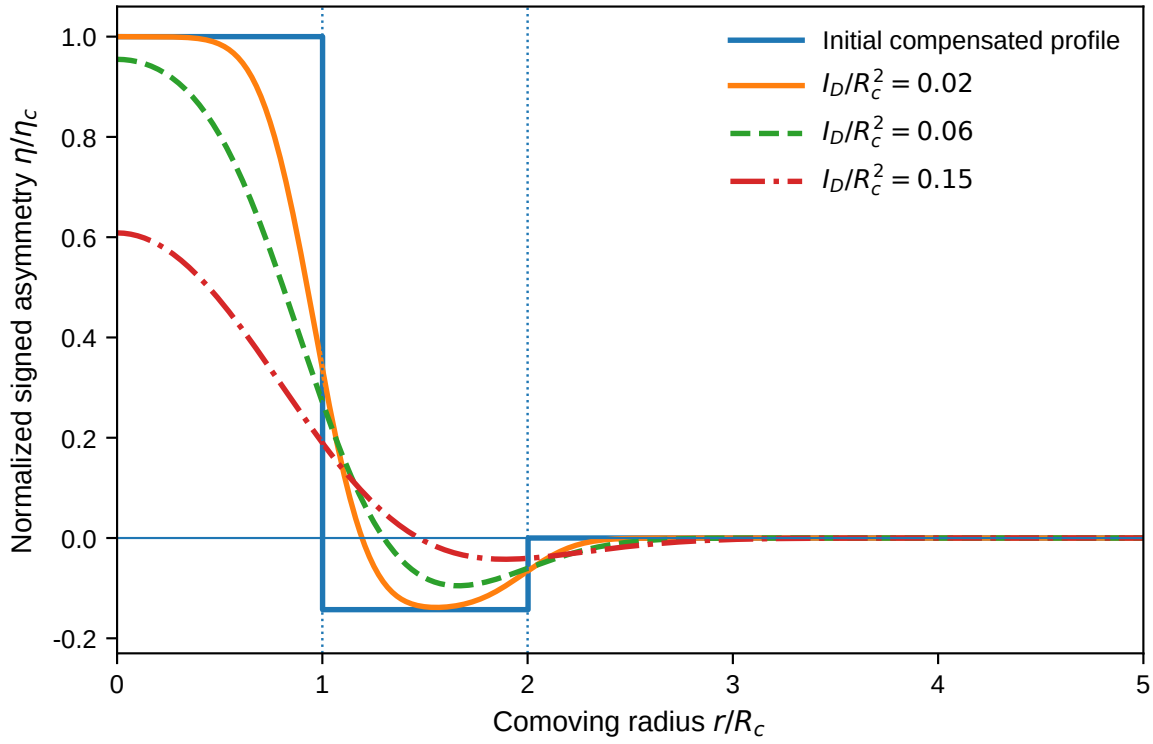



**Fig. 1** Compensated spherical profile with $R_s/R_c = 2$ and $\eta_s/\eta_c = -1/7$. The initial core-shell profile is compared with its heat-kernel evolution at three accumulated diffusion times $I_D/R_c^2$

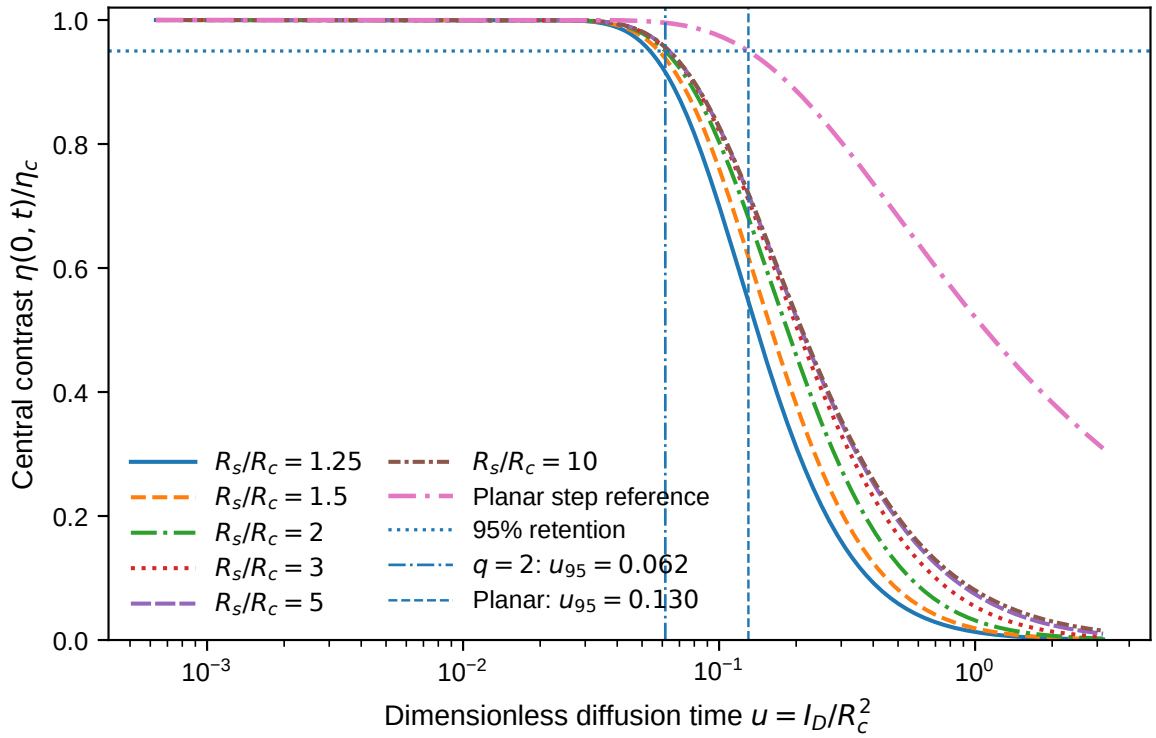



**Fig. 2** Central contrast as a function of dimensionless diffusion time for several compensated shell-to-core radius ratios. The planar step is shown as a reference

An uncompensated spherical top-hat retains a leading monopole contribution and decays at the centre as $u^{-3/2}$. In the compensated case that term is absent, so the leading central tail decays one additional power of $u$. This conclusion follows directly from the zero signed-volume integral and the finite second moment of the initial profile.

**Proposition 2** (Late-time central decay)**.** *For the compensated profile in Eq. (20) with finite $q > 1$, the leading late-time central contrast is given by Eq. (33).*

*Proof.* Expand the exponential in Eq. (31) as $1 - r'^2/(4\tau) + O(\tau^{-2})$. The integral of the constant term is $M_0 = 0$. The next term is $-M_2/(4\tau)$. Substituting Eq. (32) and writing $u = \tau/R_c^2$ gives Eq. (33). □

The asymptotic result is an analytical statement about the idealised signed profile. It does not include the feedback of annihilation products on the plasma transport coefficient, nor does it establish that the early-Universe baryon plasma reaches the asymptotic regime assumed in the expansion.

# 4 A conditional scalar-field source and abundance normalisation

The transport model requires a source for the signed baryon excess. As a conditional effective description, consider the derivative interaction

$$\mathcal{L}_{\rm int} = \frac{\partial_\mu \phi}{f} J_B^\mu, \tag{34}$$

where $\phi$ is a canonical scalar field, $f$ is a mass scale, and $J_B^\mu$ is the baryon current. Natural units $c = \hbar = k_B = 1$ are used in this section. The scalar equation contains a term proportional to the divergence of the baryon current. If baryon number were exactly conserved, the interaction could be integrated by parts into a boundary term. Baryon-number-changing reactions are therefore required for the effective bias to influence the net abundance. In a spatially homogeneous patch, the quantity

$$\mu_{\rm eff} = \frac{\dot{\phi}}{f} \tag{35}$$

may be interpreted as an effective chemical-potential bias in the small-$|\mu_{\rm eff}|/T$ limit. This interpretation is a model assumption and is not a universal consequence of Eq. (34)

[28]. For the canonical scalar action with the interaction in Eq. (34), the corresponding field equation is written as

$$\ddot{\phi} + 3H\dot{\phi} - \frac{1}{a^2}\nabla_\chi^2\phi + V'(\phi) = -\frac{1}{f}\nabla_\mu J_B^\mu. \tag{36}$$

The right-hand side represents the back-reaction associated with baryon-number violation. The benchmark below neglects it over the selected interval.

A minimal relaxation equation for the signed physical density $n_B = n_+ - n_-$ is

$$\frac{\partial n_B}{\partial t} + 3Hn_B = \frac{D}{a^2}\nabla_\chi^2 n_B - \Gamma_B(T)\left[n_B - n_B^{\rm eq}(T,\phi)\right], \tag{37}$$

where $\Gamma_B(T)$ is the baryon-number-changing reaction rate. In the relativistic-fermion, small-bias approximation, write

$$n_B^{\rm eq} = \frac{g_B}{6}\mu_{\rm eff}T^2 = \frac{g_B}{6}\frac{\dot{\phi}}{f}T^2. \tag{38}$$

The coefficient $g_B$ summarises the relevant relativistic degrees of freedom and the chemical-equilibrium constraints imposed by the chosen reaction network. Its value must be calculated for a specified particle content. Here it is retained as an illustrative effective parameter and is not identified with a derived Standard Model result.

Let $Y_B = n_B/s$, where $s = (2\pi^2/45)g_{*s}T^3$ is the entropy density. During a short freeze-out interval in which spatial transport can be neglected, entropy conservation gives

$$\dot{Y}_B = -\Gamma_B(T)\left[Y_B - Y_B^{\rm eq}(T)\right], \qquad Y_B^{\rm eq}(T) = \frac{15g_B}{4\pi^2 g_{*s}(T)}\alpha(T), \tag{39}$$

where $\alpha(T) = \dot{\phi}/(fT)$. The solution between $t_i$ and $t_f$ is

$$\begin{aligned} Y_B(t_f) =& Y_B(t_i)\exp\left[-\int_{t_i}^{t_f}\Gamma_B(u)\,{\rm d}u\right] \\ &+ \int_{t_i}^{t_f}\Gamma_B(t')Y_B^{\rm eq}(t')\exp\left[-\int_{t'}^{t_f}\Gamma_B(u)\,{\rm d}u\right]{\rm d}t'. \end{aligned} \tag{40}$$

This expression makes clear that the final yield depends on the reaction-rate history. In the sudden-freeze-out approximation, $Y_B(T_D) \simeq Y_B^{\rm eq}(T_D)$. If entropy is conserved afterwards, $\eta_{B,0} \simeq 7.04 Y_B$, and therefore

$$\eta_{B,0}^{\rm model} \simeq \frac{105.6}{4\pi^2}\frac{g_B}{g_{*s}(T_D)}\alpha_D, \qquad \alpha_D = \frac{|\dot{\phi}(T_D)|}{fT_D}. \tag{41}$$

The absolute value denotes the amplitude in the patch whose sign is being normalised. The opposite-sign patch has the opposite signed yield.

For the abundance target we use the published combined BBN and CMB determination $\eta_{B,0} = (6.120 \pm 0.038) \times 10^{-10}$ [30]. This value is used only as a normalisation target. Inverting Eq. (41) gives

$$\alpha_D^{\rm req} = \frac{4\pi^2 g_{*s}(T_D)}{105.6 g_B}\eta_{B,0} = 2.44 \times 10^{-8}\left(\frac{1}{g_B}\right)\left(\frac{g_{*s}(T_D)}{106.75}\right), \tag{42}$$

where the numerical coefficient carries the relative uncertainty of the adopted abundance. Table 2 lists illustrative values for $g_{*s} = 106.75$.

**Table 2:** Required effective source amplitude for the published baryon-to-photon normalisation. Values of $g_B$ are illustrative and do not represent a completed chemical-equilibrium calculation.

| Illustrative $g_B$ | Required $\alpha_D$ |
|---|---|
| 1 | $(2.44 \pm 0.02) \times 10^{-8}$ |
| 2 | $(1.22 \pm 0.01) \times 10^{-8}$ |
| 4 | $(6.11 \pm 0.04) \times 10^{-9}$ |
| 10 | $(2.44 \pm 0.02) \times 10^{-9}$ |

For a transparent scalar-field example, take

$$V(\phi) = \frac{1}{2}m_\phi^2\phi^2, \qquad m_\phi^2 > 0. \tag{43}$$

The potential has a single minimum at $\phi = 0$ and does not possess two degenerate vacua. It therefore does not support a stable topological wall separating two vacuum phases. The sign-changing field profile used for the benchmark is prescribed on the freeze-out slice,

$$\phi_D(x) = \Phi_D \tanh\left(\frac{x}{\ell_D}\right), \qquad \dot\phi_D(x) = -\frac{m_\phi^2}{3H_D}\phi_D(x). \tag{44}$$

The velocity is the leading slow-roll expression when $m_\phi^2 \ll H_D^2$ and the gradient force is subdominant. For $x < 0$, $\phi_D < 0$ and $\dot\phi_D > 0$, so the sign of the effective bias is opposite to that in the $x > 0$ patch. This is an imposed long-wavelength initial condition. The quadratic potential evolves the supplied configuration but does not explain how it formed.

Use the benchmark values

$$T_D = 100\ \text{GeV}, \quad g_* = g_{*s} = 106.75, \quad g_B = 4, \quad f = 10^6\ \text{GeV}, \quad \Phi_D = 10^{17}\ \text{GeV}, \tag{45}$$

and $H_D = 1.405 \times 10^{-14}$ GeV for a radiation-dominated background. Equation (42) gives $\alpha_D = 6.106 \times 10^{-9}$. Matching the magnitude of the slow-roll velocity in Eq. (44) to this value fixes

$$m_\phi^2 = \frac{3H_D f T_D \alpha_D}{\Phi_D}, \qquad m_\phi = (5.073 \pm 0.016) \times 10^{-16}\ \mathrm{GeV}, \qquad \frac{m_\phi}{H_D} = 0.0361. \tag{46}$$

The mass is calibrated to the adopted abundance. Propagating only the quoted uncertainty in $\eta_{B,0}$, with all other benchmark inputs held fixed, gives the uncertainty shown in Eq. (46). The mass is not an independent prediction of the potential.

The radiation energy density at the selected temperature is

$$\rho_R = \frac{\pi^2}{30} g_* T_D^4 = 3.512 \times 10^9\ \mathrm{GeV}^4. \tag{47}$$

The potential and kinetic energy fractions at $|\phi| = \Phi_D$ are

$$\frac{V(\Phi_D)}{\rho_R} = 3.66 \times 10^{-7}, \qquad \frac{\dot{\phi}_D^2}{2\rho_R} = 5.31 \times 10^{-11}. \tag{48}$$

For a transition width $\ell_D = 100 H_D^{-1}$, the peak gradient estimate $\rho_{\nabla,\max} \simeq \Phi_D^2/(2\ell_D^2)$ gives

$$\frac{\rho_{\nabla,\max}}{\rho_R} = 2.81 \times 10^{-8}. \tag{49}$$

The scalar sector is subdominant for this selected parameter point. These are background energy estimates, not a numerical evolution of the scalar field equation.

The scalar benchmark and the spherical transport problem serve different purposes. Equation (44) is a planar scalar initial condition used to check the effective source amplitude and its energy budget. The spherical core-shell profile in Section 4 is a separate idealised signed-asymmetry initial condition used to quantify the effect of finite geometry. No claim is made that the planar scalar profile dynamically produces the spherical core-shell configuration.

# 5 Isocurvature screening and stochastic seeding

For a light spectator scalar during quasi-de Sitter inflation, the field fluctuation per logarithmic interval is approximately $\mathcal{P}_{\delta\phi}^{1/2} = H_I/(2\pi)$ [31]. Away from the transition

surface, where $|\phi_D|$ is of order $\Phi_D$ and the local yield is proportional to $\dot{\phi} \propto \phi$, the corresponding baryon entropy perturbation is estimated as

$$\mathcal{P}_{S_{b\gamma}}^{1/2} \simeq \frac{H_I}{2\pi\Phi_D}. \tag{50}$$

This linear estimate is not valid arbitrarily close to the surface where the background field passes through zero. If cold dark matter is adiabatic and the baryons carry the only entropy perturbation, a large-scale total-matter estimate is $\mathcal{P}_{S_{m\gamma}}^{1/2} \simeq f_b \mathcal{P}_{S_{b\gamma}}^{1/2}$, where $f_b = \Omega_b/\Omega_m \simeq 0.156$ for the Planck 2018 background parameters [32].

For a transparent screening calculation, use the Planck 2018 95% upper bound $\beta_{\rm iso} < 0.038$ for an uncorrelated, scale-invariant cold-dark-matter isocurvature mode and the reference curvature amplitude $\mathcal{P}_{\mathcal{R}} = 2.1 \times 10^{-9}$ [33]. The associated reference amplitude is

$$\mathcal{P}_{S,\rm ref}^{1/2} = \left(\frac{\beta_{\rm iso}}{1-\beta_{\rm iso}}\mathcal{P}_{\mathcal{R}}\right)^{1/2} = 9.108 \times 10^{-6}. \tag{51}$$

Requiring the estimated total-matter contribution to remain below this reference gives

$$\frac{H_I}{\Phi_D} \lesssim \frac{2\pi}{f_b}\mathcal{P}_{S,\rm ref}^{1/2} = 3.668 \times 10^{-4}. \tag{52}$$

For $\Phi_D = 10^{17}$ GeV this corresponds to $H_I \lesssim 3.67 \times 10^{13}$ GeV. At $H_I = 10^{13}$ GeV, Eq. (50) gives a baryon entropy amplitude of $1.59 \times 10^{-5}$ and a weighted total-matter amplitude of $2.48 \times 10^{-6}$, approximately 0.27 of the reference amplitude.

Equation (52) is a screening proxy, not a Planck likelihood constraint on a pure baryon-isocurvature model. Baryon and cold-dark-matter isocurvature modes have different transfer functions and acoustic signatures. A baryon-specific analysis would be needed for a quantitative comparison with CMB observations [34]. The use of the CDM bound here is restricted to an order-of-magnitude check of the benchmark. The relation between the fluctuation ratio and the adopted screening amplitude is plotted in Fig. 3.

If the spectator remains light and classical drift is neglected, independent inflationary increments over $N$ e-fold intervals give the optimistic random-walk estimate

$$\sigma_\phi(N) \simeq \frac{H_I}{2\pi}\sqrt{N}. \tag{53}$$

Combining this expression with Eq. (52), the rms excursion obeys

$$\frac{\sigma_\phi(N)}{\Phi_D} \lesssim \frac{3.668 \times 10^{-4}}{2\pi}\sqrt{N}. \tag{54}$$

An rms excursion of order $\Phi_D$ would require

$$N \gtrsim N_{\rm req} = \left(\frac{2\pi}{3.668 \times 10^{-4}}\right)^2 \simeq 2.93 \times 10^8. \tag{55}$$

For $N = 60$, the same estimate gives

$$\frac{\sigma_\phi(60)}{\Phi_D} \lesssim 4.52 \times 10^{-4}. \tag{56}$$

The result is far below the order-unity field excursion assumed in Eq. (44). It is a consistency check for an unbiased random walk under the stated screen, not an exclusion of all inflationary histories. It neglects mass-induced suppression, classical drift, correlations between scales, and any earlier classical field configuration. The dependence of the estimated rms excursion on the number of e-fold intervals is shown in Fig. 4.

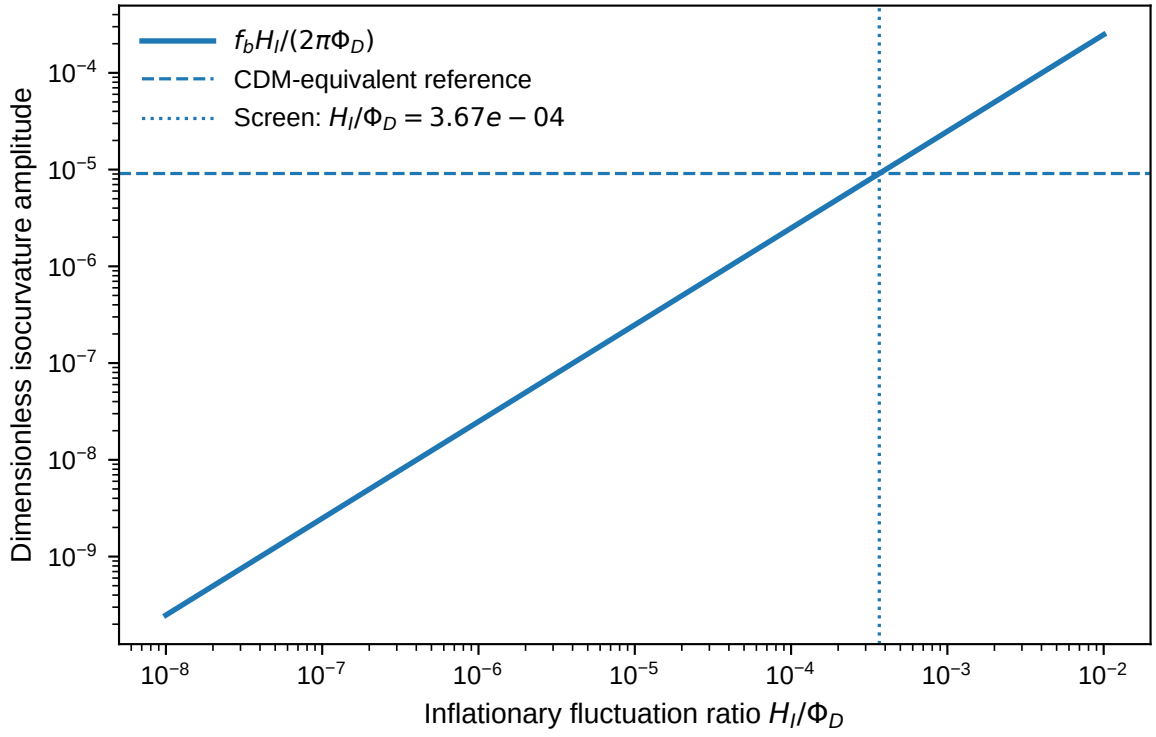



**Fig. 3** Approximate isocurvature screening for the benchmark field amplitude. The horizontal line denotes the cold-dark-matter-equivalent reference amplitude. This comparison is not a baryon-isocurvature likelihood fit

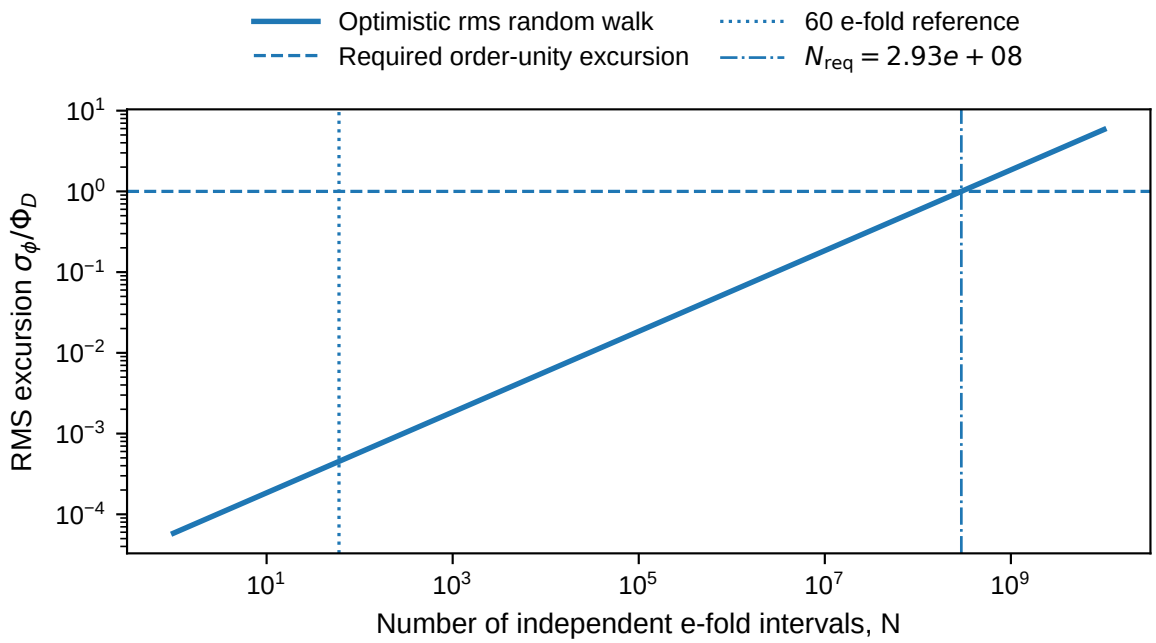



**Fig. 4** Optimistic stochastic field excursion divided by the assumed field amplitude. The 60-e-fold reference lies well below unity under the adopted screening proxy

# 6 Observational implications and tests

The analytical conditions derived above are necessary transport checks. They are not sufficient to establish a viable cosmological model. Several further calculations would be required before a particular compensated-domain scenario could be compared directly with observations.

During Big Bang nucleosynthesis, diffusion of baryons and antibaryons toward an interface could lead to annihilation and energy injection. The resulting light-element yields depend on the domain size distribution, transport coefficients, annihilation history, and thermal evolution. Earlier analyses have shown that nucleosynthesis can constrain matter-antimatter configurations [14–16]. The present paper does not evolve a BBN reaction network, so it does not claim that the benchmark has passed those constraints.

Annihilation at matter-antimatter boundaries can produce energetic photons and secondary particles. A predicted gamma-ray signal depends on interface area, baryon density, relative velocity, distance, redshift, and radiative transfer. Observations already restrict nearby matter-antimatter admixtures and candidate antimatter objects [20, 21]. Since the domain geometry and environment have not been specified at the level needed for a flux calculation, no absolute gamma-ray flux is quoted here.

The cosmic microwave background can constrain both isocurvature perturbations and energy injection. The calculation in Section 6 uses a cold-dark-matter-equivalent

amplitude only as a screening reference. It is not a replacement for a baryon-specific transfer calculation or a likelihood evaluation. Likewise, antideuteron and antihelium observations would require modelling secondary production, acceleration, and propagation before they could be connected to primordial domains [22, 23]. No reported antinucleus candidate is treated here as evidence for a primordial antimatter reservoir.

The main tests and their present status are summarised in Table 3.

**Table 3:** Tests required for a physical realisation of the compensated-domain hypothesis.

| Test | Requirement for a viable model | Present status in this study |
|---|---|---|
| Microphysical source | Derive $\Gamma_B(T)$, $g_B$, and the signed source from a specified particle-physics model. | Effective relaxation closure and illustrative susceptibility only. |
| Transport | Calculate $D(T)$ and evaluate the integrated diffusivity over the relevant thermal history. | Exact analytical criteria are derived; the plasma transport law is not supplied. |
| BBN | Evolve the domain distribution and annihilation history through a nuclear reaction network. | Not performed. |
| CMB | Compute baryon-isocurvature transfer functions and energy injection, then compare with likelihoods. | CDM-equivalent screening proxy only. |
| Gamma rays | Specify the interface geometry and environment and calculate the emitted and propagated spectrum. | No absolute flux calculation. |
| Cosmic antinuclei | Model secondary backgrounds, source spectra, and propagation before interpreting a candidate signal. | No antinucleus prediction is made. |

# 7 Discussion and limitations

The main result of the transport analysis is that the geometry of a compensated profile affects how its central signed contrast is retained. The planar step provides an exact one-dimensional reference. A finite spherical core-shell profile has an exact three-dimensional convolution, and its 95% retention threshold depends on the shell-to-core radius ratio. For the example $R_s/R_c = 2$, the allowed dimensionless diffusion time is less than half the planar value. The reason is not a change in the microscopic diffusion coefficient. It is the geometric effect of diffusion in three directions together with the opposite-sign compensation shell.

A second consequence is the late-time suppression of the central contrast. The zero monopole moment removes the $u^{-3/2}$ contribution that would occur for an uncompensated finite sphere. The leading term is set by the second radial moment and decays as $u^{-5/2}$. This result is useful when comparing finite compensated profiles, but it is not a prediction for the actual early-Universe plasma until the function $D(t)$ is calculated for a specified particle content and thermal history.

The scalar-field calculation is intentionally conditional. The derivative coupling does not provide a complete baryogenesis model without baryon-number violation and a consistent chemical-equilibrium treatment. The susceptibility coefficient and reaction rate are not derived from a specified microscopic theory. The benchmark mass is inferred after normalising the source to the observed abundance. It should therefore be read as a parameter value required by the selected assumptions, not as a prediction. The quadratic potential has one minimum, and the sign-changing initial profile is supplied by hand. The stochastic estimate further shows that the adopted 60-e-fold light-field random walk does not generate the assumed amplitude while satisfying the approximate isocurvature screen.

Several limitations remain. First, the signed-density equation removes the direct pair-annihilation term by construction. The finite-sphere solution therefore describes the diffusion of signed contrast, not the full coupled evolution of the individual baryon and antibaryon populations near a reactive interface. Second, the top-hat core-shell profile is an idealisation. A smooth profile can be treated by convolving it with the same heat kernel, but its quantitative retention threshold will depend on the chosen transition shape. Third, the transport coefficient and annihilation rate have not been derived from early-Universe plasma microphysics. Fourth, no BBN network, baryon-specific CMB likelihood, or quantitative gamma-ray calculation has been carried out. Finally, no dynamics is supplied that generates the long-wavelength initial condition. These

omissions prevent the model from being presented as an explanation of the cosmic matter-antimatter asymmetry.

The conclusions are consequently limited to the stated mathematical and benchmark results. A globally compensated signed distribution can contain local regions of opposite asymmetry. Its subsequent smoothing can be calculated analytically for the planar step and for the spherical core-shell profile considered here. Whether such a profile forms and survives in the physical universe remains an open question requiring microphysical calculations and a fully specified cosmological history.

# 8 Conclusion

This paper has examined the transport of compensated baryon-asymmetry profiles in an expanding FLRW background. The signed-density equation conserves the integrated asymmetry when there is no boundary flux and the net signed source integrates to zero. After the source switches off, the accumulated comoving diffusivity determines the smoothing of the profile. Beyond the standard planar reference solution, an exact three-dimensional heat-kernel expression has been obtained for a finite compensated spherical core surrounded by an opposite-sign shell. The central-contrast threshold depends on the shell-to-core radius ratio. For $R_s/R_c = 2$, 95% central retention requires $I_D/R_c^2 \leq 0.06164$. At late times, compensation removes the leading monopole contribution and the central contrast decays as $u^{-5/2}$. A conditional derivative-coupled scalar benchmark has also been normalised to the published baryon-to-photon ratio. For the selected parameters, the inferred scalar mass is $(5.073 \pm 0.016) \times 10^{-16}$ GeV, where the uncertainty reflects only the quoted baryon-to-photon normalisation, and the scalar energy remains subdominant. The isocurvature and stochastic calculations are approximate consistency screens. The work therefore provides an analytical test of transport and a clearly delimited scalar-source benchmark.

# Statements and Declarations

**Funding.** This research received no specific grant from any funding agency in the public, commercial, or not-for-profit sectors.

**Competing interests.** The author declares that there are no competing financial or non-financial interests that could have influenced the work reported in this manuscript.

**Author contributions.** Syed Eirfan Atthar: Conceptualization, methodology, mathematical formulation, formal analysis, software, visualization, and writing of the original draft. The author is responsible for the scientific interpretation and final manuscript version.

**Ethics approval and consent to participate.** Not applicable. This theoretical study does not involve human participants, identifiable personal data, or animal subjects.

**Consent for publication.** Not applicable.

**Data availability.** No observational or secondary datasets were used in this study. The numerical results were generated from the analytical expressions and parameter values stated in the manuscript. The numerical retention thresholds are provided in Online Resource and are also archived with the reproducibility software record on Zenodo.

**Code availability.** The Python software used to calculate the spherical retention thresholds, compare the heat-kernel expression with direct radial quadrature, and generate the figures is publicly archived on Zenodo as a version-specific record (Zenodo record; [35]). The archived software includes the source script, its requirements, documentation, licence, and numerical retention table. The script reads no observational data files and requires Python 3.10 or later, NumPy, SciPy, and Matplotlib.

**Supplementary information.** Online Resource contains the Python script used for the analytical calculations, numerical checks and figure generation and contains the numerical 95% central-contrast thresholds, including the planar reference.

**Use of generative AI.** Strictly no Generative AI was used for editorial support, manuscript restructuring, literature search, discussion of analytical approaches, assistance in formulating neither checking candidate mathematical extension, Python code drafting or language editing. The author is responsible for verifying all works independently including the derivations, numerical results, literature, methods, references, physical interpretations and final manuscript submit.

# References


[1] LHCb Collaboration, Observation of charge-parity symmetry breaking in baryon decays, *Nature* **643**, 1223-1228 (2025). https://doi.org/10.1038/s41586-025-09119-3.

[2] M. Sarrazin, Braneworld baryogenesis and QCD-era magnetogenesis: a predictive link, *Eur. Phys. J. C* **86**, 801 (2026). https://doi.org/10.1140/epjc/s10052-026-16069-1.

[3] A. D. Sakharov, Violation of CP invariance, C asymmetry, and baryon asymmetry of the universe, *Sov. Phys. Usp.* **34**, 392-393 (1991), reprint of the 1967 original. https://doi.org/10.1070/PU1991v034n05ABEH002497.

[4] V. A. Kuzmin, V. A. Rubakov, and M. E. Shaposhnikov, On anomalous electroweak baryon-number non-conservation in the early universe, *Phys. Lett. B* **155**, 36-42 (1985). https://doi.org/10.1016/0370-2693(85)91028-7.

[5] I. Affleck and M. Dine, A new mechanism for baryogenesis, *Nucl. Phys. B* **249**, 361-380 (1985). https://doi.org/10.1016/0550-3213(85)90021-5.

[6] M. Dine and A. Kusenko, The origin of the matter-antimatter asymmetry, *Rev. Mod. Phys.* **76**, 1-30 (2004). https://doi.org/10.1103/RevModPhys.76.1.

[7] A. G. Cohen and D. B. Kaplan, Thermodynamic generation of the baryon asymmetry, *Phys. Lett. B* **199**, 251-258 (1987). https://doi.org/10.1016/0370-2693(87)91369-4.

[8] A. G. Cohen, D. B. Kaplan, and A. E. Nelson, Progress in electroweak baryogenesis, *Annu. Rev. Nucl. Part. Sci.* **43**, 27-70 (1993). https://doi.org/10.1146/annurev.ns.43.120193.000331.

[9] S. Davidson, E. Nardi, and Y. Nir, Leptogenesis, *Phys. Rep.* **466**, 105-177 (2008). https://doi.org/10.1016/j.physrep.2007.12.001.

[10] V. A. Kuzmin, M. E. Shaposhnikov, and I. I. Tkachev, Matter-antimatter domains in the universe: a solution of the vacuum walls problem, *Phys. Lett. B* **105**, 167-170 (1981). https://doi.org/10.1016/0370-2693(81)91013-3.

[11] A. D. Dolgov and J. Silk, Baryon isocurvature fluctuations at small scales and baryonic dark matter, *Phys. Rev. D* **47**, 4244-4255 (1993). https://doi.org/10.1103/PhysRevD.47.4244.

[12] M. Yu. Khlopov, S. G. Rubin, and A. S. Sakharov, Possible origin of antimatter regions in the baryon dominated universe, *Phys. Rev. D* **62**, 083505 (2000). https://doi.org/10.1103/PhysRevD.62.083505.

[13] A. G. Cohen, A. De Rújula, and S. L. Glashow, A matter-antimatter universe? *Astrophys. J.* **495**, 539-549 (1998). https://doi.org/10.1086/305328.

[14] J. B. Rehm and K. Jedamzik, Big bang nucleosynthesis with matter-antimatter domains, *Phys. Rev. Lett.* **81**, 3307-3310 (1998). https://doi.org/10.1103/PhysRevLett.81.3307.

[15] J. B. Rehm and K. Jedamzik, Limits on cosmic matter-antimatter domains from big bang nucleosynthesis, *Phys. Rev. D* **63**, 043509 (2001). https://doi.org/10.1103/PhysRevD.63.043509.

[16] H. Kurki-Suonio and E. Sihvola, Constraining antimatter domains in the early universe with big bang nucleosynthesis, *Phys. Rev. Lett.* **84**, 3756-3759 (2000). https://doi.org/10.1103/PhysRevLett.84.3756.

[17] A. D. Dolgov, S. I. Godunov, A. S. Rudenko, and I. I. Tkachev, Separated matter and antimatter domains with vanishing domain walls, *JCAP* **10**, 027 (2015). https://doi.org/10.1088/1475-7516/2015/10/027.

[18] A. D. Dolgov, S. I. Godunov, and A. S. Rudenko, Evolution of thick domain walls in inflationary and $p = w\rho$ universe, *Eur. Phys. J. C* **78**, 855 (2018). https://doi.org/10.1140/epjc/s10052-018-6350-7.

[19] J. Rafelski, J. Birrell, A. Steinmetz, and C. T. Yang, A short survey of matter-antimatter evolution in the primordial Universe, *Universe* **9**, 309 (2023). https://doi.org/10.3390/universe9070309.

[20] D. A. Prokhorov, Upper bounds on matter-antimatter admixture from gamma-ray observations of colliding clusters of galaxies with the Fermi Large Area Telescope, *Phys. Rev. D* **91**, 083002 (2015). https://doi.org/10.1103/PhysRevD.91.083002.

[21] S. Dupourqué, L. Tibaldo, and P. von Ballmoos, Constraints on the antistar fraction in the Solar System neighborhood from the 10-year Fermi Large Area Telescope gamma-ray source catalog, *Phys. Rev. D* **103**, 083016 (2021). https://doi.org/10.1103/PhysRevD.103.083016.

[22] V. Poulin, P. Salati, I. Cholis, M. Kamionkowski, and J. Silk, Where do the AMS-02 antihelium events come from? *Phys. Rev. D* **99**, 023016 (2019). https://doi.org/10.1103/PhysRevD.99.023016.

[23] M. A. Fedderke, D. E. Kaplan, A. Mathur, S. Rajendran, and E. H. Tanin, Fireball antinucleosynthesis, *Phys. Rev. D* **109**, 123028 (2024). https://doi.org/10.1103/PhysRevD.109.123028.

[24] S. Weiss, A. I. Dembitskaia, M. Krasnov, M. Yu. Khlopov, and S. Yadav, Asymmetric antimatter evolution in baryon asymmetrical universe, *Symmetry* **18**(10), 1686 (2026). https://doi.org/10.3390/sym18101686.

[25] M. Yu. Khlopov and O. M. Lecian, The formalism of Milky-Way antimatter-domains evolution, *Galaxies* **11**(2), 50 (2023). https://doi.org/10.3390/galaxies11020050.

[26] M. Yu. Khlopov and O. M. Lecian, Effects of baryon-antibaryon annihilation in the evolution of antimatter domains in baryon asymmetrical Universe, *Phys. Sci. Forum* **2**(1), 31 (2021). https://doi.org/10.3390/ECU2021-09267.

[27] J. Crank, *The Mathematics of Diffusion*, 2nd edn. (Oxford University Press, Oxford, 1975).

[28] A. Dasgupta, R. K. Jain, and R. Rangarajan, Effective chemical potential in spontaneous baryogenesis, *Phys. Rev. D* **98**, 083527 (2018). https://doi.org/10.1103/PhysRevD.98.083527.

[29] E. K. Anderson et al. (ALPHA Collaboration), Observation of the effect of gravity on the motion of antimatter, *Nature* **621**, 716-722 (2023). https://doi.org/10.1038/s41586-023-06527-1.

[30] T.-H. Yeh, K. A. Olive, B. D. Fields, E. Aver, R. W. Pogge, N. S. J. Rogers, E. D. Skillman, and M. K. Weller, The LBT $Y_p$ Project. V. Cosmological implications of a new determination of primordial $^4$He, *Astrophys. J.* **1008**(2), 241 (2026). https://doi.org/10.3847/1538-4357/ae879c.

[31] V. F. Mukhanov, H. A. Feldman, and R. H. Brandenberger, Theory of cosmological perturbations, *Phys. Rep.* **215**, 203-333 (1992). https://doi.org/10.1016/0370-1573(92)90044-Z.

[32] N. Aghanim et al. (Planck Collaboration), Planck 2018 results. VI. Cosmological parameters, *Astron. Astrophys.* **641**, A6 (2020). https://doi.org/10.1051/0004-6361/201833910.

[33] Y. Akrami et al. (Planck Collaboration), Planck 2018 results. X. Constraints on inflation, *Astron. Astrophys.* **641**, A10 (2020). https://doi.org/10.1051/0004-6361/201833887.

[34] N. Lee and Y. Ali-Haïmoud, Probing small-scale baryon and dark matter isocurvature perturbations with cosmic microwave background anisotropies, *Phys. Rev. D* **104**, 103509 (2021). https://doi.org/10.1103/PhysRevD.104.103509.

[35] S. E. Atthar, *Reproducibility code for compensated baryon-asymmetry transport*, Zenodo (2026). https://doi.org/10.5281/zenodo.23858385.